

ACCEPTED MANUSCRIPT

Evolution of nanomechanical properties and crystallinity of individual titanium dioxide nanotube resonators

To cite this article before publication: Stefano Stassi *et al* 2017 *Nanotechnology* in press <https://doi.org/10.1088/1361-6528/aaa46c>

Manuscript version: Accepted Manuscript

Accepted Manuscript is “the version of the article accepted for publication including all changes made as a result of the peer review process, and which may also include the addition to the article by IOP Publishing of a header, an article ID, a cover sheet and/or an ‘Accepted Manuscript’ watermark, but excluding any other editing, typesetting or other changes made by IOP Publishing and/or its licensors”

This Accepted Manuscript is © 2017 IOP Publishing Ltd.

During the embargo period (the 12 month period from the publication of the Version of Record of this article), the Accepted Manuscript is fully protected by copyright and cannot be reused or reposted elsewhere.

As the Version of Record of this article is going to be / has been published on a subscription basis, this Accepted Manuscript is available for reuse under a CC BY-NC-ND 3.0 licence after the 12 month embargo period.

After the embargo period, everyone is permitted to use copy and redistribute this article for non-commercial purposes only, provided that they adhere to all the terms of the licence <https://creativecommons.org/licenses/by-nc-nd/3.0>

Although reasonable endeavours have been taken to obtain all necessary permissions from third parties to include their copyrighted content within this article, their full citation and copyright line may not be present in this Accepted Manuscript version. Before using any content from this article, please refer to the Version of Record on IOPscience once published for full citation and copyright details, as permissions will likely be required. All third party content is fully copyright protected, unless specifically stated otherwise in the figure caption in the Version of Record.

View the [article online](#) for updates and enhancements.

Evolution of nanomechanical properties and crystallinity of individual titanium dioxide nanotube resonators

Stefano Stassi^{a,b,*,‡}, Andrea Lamberti^{a,b,‡}, Ignazio Roppolo^b, Alberto Casu^c, Stefano Bianco^a, Davide Scaiola^a, Andrea Falqui^c, Candido Fabrizio Pirri^{a,b}, Carlo Ricciardi^a

^a Department of Applied Science and Technology, Politecnico di Torino, Corso Duca degli Abruzzi 24, 10129 Torino, Italy

^b Center for Sustainable Future Technologies, Istituto Italiano di Tecnologia, Corso Trento 21, Torino, 10129 Italy

^c King Abdullah University of Science and Technology (KAUST), Biological and Environmental Sciences and Engineering (BESE) Division, Nabla Lab, Thuwal 23955-6900, Saudi Arabia.

[‡]These authors equally contributed to the work

*Corresponding authors: stefano.stassi@polito.it

ABSTRACT

Herein a complete characterization of single TiO₂ nanotube resonator was reported for the first time. The modal vibration response analysis allows a non-invasive indirect evaluation of the mechanical properties of the TiO₂ nanotube. The effect of post-grown thermal treatments on nanotube mechanical properties was investigated and carefully correlated to the chemico-physical parameters evolution. The Young's modulus of TiO₂ nanotube linearly rises from 57 GPa up to 105 GPa for annealing at 600°C depending on the compositional and crystallographic evolution of the

1
2
3 nanostructure. Considering the growing interest in single nanostructure devices, the reported
4
5 findings allow a deeper understanding of the properties of individual titanium dioxide nanotubes
6
7 extrapolated from their standard arrayed architecture.
8
9

10
11
12
13
14 KEYWORDS: nanomechanical resonator, TiO₂ nanotubes, Young's modulus, crystallization,
15
16 mechanical properties.
17
18
19
20
21

22 INTRODUCTION

23
24
25 Since the first report of Grimes et al.[1] in 2001, the growth of self-organized TiO₂ nanotube (NT)
26
27 arrays by electrochemical anodic oxidation of titanium surface has increasingly attracted great
28
29 scientific interest in recent years owing to their exceptional properties, peculiar arrangement, and
30
31 potential for almost every research field.
32
33

34
35 Vertically-oriented TiO₂ NT arrays can provide high surface area and superior electron transport
36
37 properties that, coupled to the highly ordered architecture, allow their effective exploitation for
38
39 several class of devices such as solar cells (dye-sensitized, solid state and perovskites solar cell),[2-
40
41 5] water splitting,[6, 7] energy storage (batteries and supercapacitors),[8, 9] sensors (UV, gas,
42
43 molecule, or pH),[10-12] electrochromic devices,[13] photocatalytic reactors,[14] memristors,[15]
44
45 cell adhesion substrates,[16] photonic devices [17] and many others.[18]
46
47

48
49 Moreover, their as-grown amorphous nature permits subsequent crystallization in the desired
50
51 polycrystalline phase, according to the application, by thermal or water-assisted post processing
52
53 treatments.[19, 20] Besides, the morphology was shown to have a strong dependence on the
54
55 crystallization procedure. Indeed, thermal treatments induce an increase of the crystallite size and
56
57 the formation of grain boundaries along the tube wall, while wet approaches can lead to a
58
59 transformation from nanotubes to porous nanorod.
60

1
2
3 Apart from the electronic and chemical properties, these structural variations can strongly influence
4 the mechanical properties of the TiO₂ nanotubes, whose variation is even more important
5 considering the strong interest for the application of metal-oxide nanostructure in flexible
6 devices.[21-23]
7
8
9

10
11
12 Generally nanostructured materials present quite different mechanical properties when compared
13 with their bulk counterparts.[24, 25] So far mechanical properties of TiO₂ nanotubes have been
14 investigated only with direct compressive measurements. Most of the analyses were performed on
15 nanotubes array by means of nanoindentation approach, where a rigid nanometric tip is pressed on
16 the top surface of the material while the applied force and deformation of the nanotubes are
17 recorded[26-31]. Young's modulus values obtained with this technique were very scattered, ranging
18 from 36-43 GPa[28] up to 80-95 GPa[31], because of the non-uniform shape of the nanostructured
19 arrays. As well, only few works measured the mechanical properties of individual TiO₂
20 nanotubes[32, 33]. Shokuhfar *et al.* compressed individual nanotubes up to fracture with the tip of
21 an atomic force microscope microcantilever inside a transmission electron microscope (TEM)[32].
22 These experiments lead to Young's modulus in the range of 23-44 GPa, comparable with the results
23 obtained from the arrays analysis, but showing a higher variability determined by the slight
24 difference in nanotube geometry. A similar approach was used by Kang *et al.* performing
25 compressive tests in a TEM using a nanoindentation holder and obtaining significantly lower values
26 (2.2-9.4 GPa)[33]. The main limitation of both approaches is that, being direct invasive methods,
27 they strongly depend on the experimental set-up and analyze only the compressive properties of the
28 material. Furthermore, the samples are usually brought to fracture and destroyed, limiting the
29 possibility of parametric analysis of the mechanical properties, such as their dependence on
30 temperature, atmosphere or crystallization phase.
31
32
33
34
35
36
37
38
39
40
41
42
43
44
45
46
47
48
49
50
51
52
53
54

55
56 In this work, we investigated the Young's modulus of single TiO₂ nanotubes with a non-invasive
57 indirect approach based on modal vibration response analysis of the inorganic nanostructure. Treacy
58 *et al.* were the first to apply this method to measure Young's modulus of individual
59
60

1
2
3 nanostructures[34]. They evaluated the vibration of individual free-standing carbon nanotubes
4 induced by thermal motion by TEM imaging and unveiled the elastic properties measuring their
5 resonance frequencies. Similarly, here we calculate Young's modulus from the measurements of
6 resonance frequency of suspended TiO₂ nanotubes. Moreover, for the first time the mechanical
7 properties of single nanotubes were measured after different thermal treatments, evaluating their
8 variation induced by crystalline structure evolution and organic compounds removal.
9
10
11
12
13
14
15
16
17
18
19

20 METHODS

21
22
23 The nanotubes were prepared by anodic oxidation of titanium foils (thickness 250 μm, 99.96%
24 purity, Goodfellow) cleaned by ultra-sonication in acetone and soft HF etching to remove native
25 oxide. The electrochemical process was conducted at 25 °C in an electrolytic solution containing
26 0.5 wt.% NH₄F and 2.5 wt.% deionized water in ethylene glycol, using a platinum sheet as counter
27 electrode (thickness 250 μm, 99.99% purity, Goodfellow). The anodization time was fixed to 30
28 minutes working under continuous stirring with a constant voltage of 60 V in order to obtain
29 nanotubes with length of approximately 10 μm. The samples were then rinsed in DI-water, dried
30 and detached by ultra-sonication in ethanol for 5 minutes. Then, a droplet of the solution containing
31 detached single nanotubes was spread on a silicon die presenting a rectangular opening over the
32 whole wafer thickness.
33
34
35
36
37
38
39
40
41
42
43
44
45

46 Vibration analysis was performed with a Laser Doppler Vibrometer (LDV) system (MSA-500,
47 Polytec GmbH). The LDV system is composed by an optical microscope with objective up to 100X
48 used to find the suspended nanotubes arranged on the edge of the opening and then to focus the
49 laser on their tip. The sample was mounted on a piezodisk used for the actuation, inside a vacuum
50 chamber, evacuated by a membrane and a turbomolecular pump (MINI-Task System, Varian Inc.
51 Vacuum Technologies) up to a vacuum level of 2×10^{-7} mbar. The sample was mechanically actuated
52 by sending an electrical signal to the piezodisk composed of a combination of sine waves with the
53
54
55
56
57
58
59
60

1
2
3 frequencies of the range under investigation. The laser light reflected by the sample, coupled with
4 the tip displacement velocity of the nanotube, exploits a shift in frequency because of Doppler
5 effect. Then, from the measurement of the laser frequency shift, the system computes the vibration
6 velocity and amplitude of the sample as function of the actuation frequency.
7
8
9

10
11
12 Differential scanning calorimetry (DSC) experiment was performed using a Netzsch DSC 204 F1
13 Phoenix instrument, equipped with a low temperature probe. The experiment was performed in air
14 (20 ml/min), scanning the temperature range between 30 °C and 600 °C with a temperature ramp
15 rate of 1°C/min and 4 isothermal steps of 1 hour each (150 °C, 300°C, 450°C and 600°C) during the
16 measurement. The same temperature program was used for thermogravimetric analysis (TGA),
17 which was performed using a Netzsch TG 209 F1 Libra instrument.
18
19
20
21
22
23
24
25

26
27 Raman characterizations on few nanotubes bundles were performed with a Renishaw inVia Reflex
28 micro-Raman spectrophotometer, equipped with a cooled CCD camera. Samples were excited at a
29 100x magnification with an Ar–Kr laser source with a wavelength of 514.5 nm.
30
31
32
33

34
35 High Resolution Transmission Electron Microscopy: High Resolution TEM (HRTEM) analysis was
36 performed ex situ on a 300 kV Cs Image corrected FEI Titan Cube microscope, studying the
37 structural evolution of the TiO₂ nanotubes against temperature after each ex situ heating step. The
38 ex situ heating was performed in air using the Wildfire system by DENSSolutions, acquiring
39 HRTEM images in the temperature range between RT (room temperature, i.e. 20°C) and 450°C.
40 This was divided in 150°C-wide steps and, for each step, a 150°C-wide heating ramp with a 1°C/min
41 rate was set; the target temperature was maintained for 3 minutes before fast decreasing the
42 temperature to RT and proceeding with the HRTEM analysis. Initial temperatures (for T>RT) were
43 reached via fast “pre-heating” temperature ramps before starting the actual 1°C/min heating ramps.
44 The heating in air caused a progressive degradation of the MEMS chip in terms of overall cleanness
45 of the thin film and of its mechanical stability, until a massive rupture of the film was observed at
46 450°C, which made impossible any further heating. Thus, 450°C was deemed as the final
47 temperature for ex situ heating experiments.
48
49
50
51
52
53
54
55
56
57
58
59
60

RESULTS AND DISCUSSION

The anodic oxidation of titanium foils in an electrolytic solution containing 0.5 wt.% NH_4F and 2.5 wt.% deionized water in ethylene glycol results in the formation of the self-organized vertically oriented TiO_2 nanotubes, as shown in Figure 1a. The selected anodization time and voltage lead to nanotubes with length of approximately 10 μm and average inner diameter of 80 nm. In order to obtain the desired suspended single nanotube, the experimental steps schematically represented in Figure 1b-e have been carried out. The as-grown NTs were rinsed in deionized water, dried and detached by ultra-sonication in ethanol for 5 minutes. A droplet of nanotube solution was dropped over a silicon die presenting a rectangular opening over the whole wafer thickness prepared by standard microfabrication technique based on KOH silicon wet etching[35]. Some of the single nanotubes spread over the whole surface with a certain amount arranged on the edge of the opening, as shown in the FESEM images reported in Figure 1f. Resonance frequency of the suspended nanotubes was evaluated as a function of the performed thermal treatments (see Figure 1g) by means of a Laser Doppler Vibrometer (LDV) which does not imply a direct measurement of the vibration amplitude, like in the classic optical lever technique, but exploits a Fast Fourier Transform approach[36]. Natural resonance frequencies of individual suspended nanotubes were measured on just spotted samples and then after each of 4 thermal treatments consisted of a heating ramp at 1°C/min and isothermal step of 1h at 150, 300, 450 and 600 °C, respectively (Figure 2a). Since the nanotubes are randomly dispersed over the sample, they can arrange in position not perfectly perpendicular to the silicon edge, even if NTs with angle above 75° were considered. The effect of the tilting angle of the suspended TiO_2 nanotubes was evaluated by a finite element simulation (results in the Supporting Information) and resulted in a variation below 0.2% for angle up to 30° with respect to the edge of the wafer. This variation is far below the frequency shifts induced by thermal annealing steps and thus was neglected in the following Young's modulus computation.

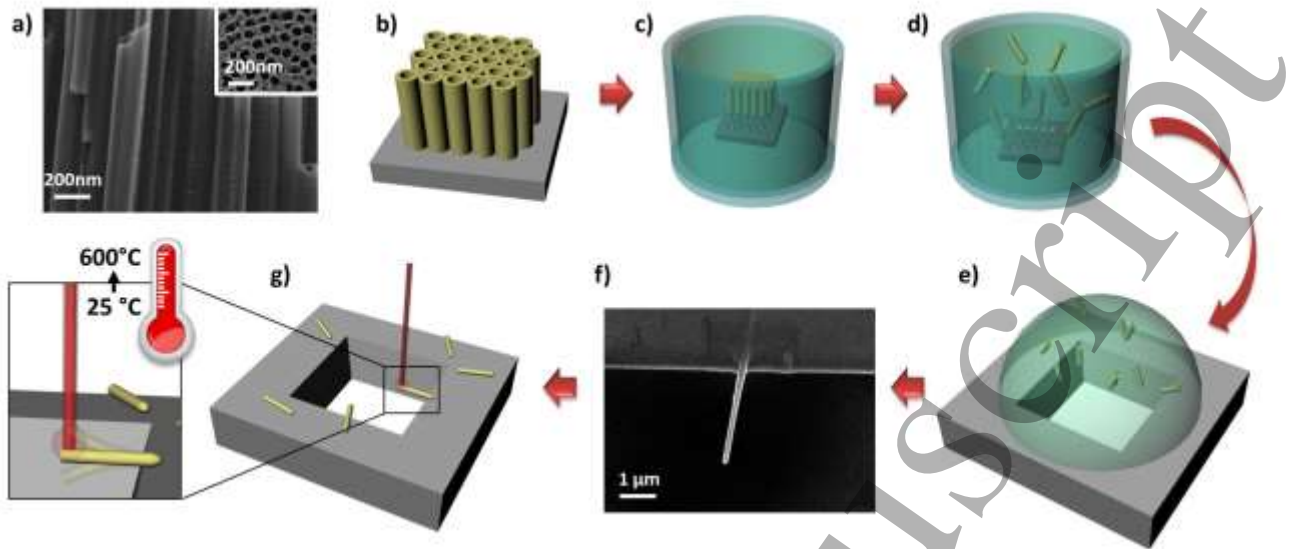


Figure 1. Scheme of the experimental procedure: cross section and top (in the inset) FESEM images of the as grown TiO_2 NTs carpet (a), the NTs sample were then cut (b), immersed in aqueous solution (c) and sonicated to detach single nanotubes (d). The dispersion was dispensed on ad-hoc designed silicon chip and let dry overnight (e) resulting in single NTs arrange on the edge of the opening (f). The chip was mounted in the vibrometer set-up for resonating measurements (g).

Simplified continuum models from the Bernoulli-Euler beam theory were used to describe the motion of the suspended TiO_2 nanotubes and to indirectly determine their elastic modulus from the natural resonance frequency. In the limit of small deformations, as well as negligible dumping effects and external forces, the equation describing the flexural motion of a beam (i.e. TiO_2 NT) is:

$$EI \frac{\partial^4 u}{\partial x^4} + \rho A \frac{\partial^2 u}{\partial t^2} = 0 \quad (1)$$

where E indicates Young's modulus, I is the moment of inertia of the beam cross-sectional area A , u is the beam displacement and ρ is the density of the beam material. Then, the natural frequency of the n^{th} mode of vibration of the beam is:

$$f_n = \frac{(k_n L)^2}{2\pi L^2} \sqrt{\frac{EI}{\rho A}} \quad (2)$$

where L is the beam length and $k_n L$ the eigenvalue for the n^{th} mode depending on the boundary conditions applied to the model. In the case of single clamped beam like the nanotubes, the eigenvalues for the first two modes are $k_1 L = 1.875$ and $k_2 L = 4.694$. For a cylindrical tube of outside and inside radii R_o and R_i the moment of inertia is $I = \pi(R_o^4 - R_i^4)$ and thus we can derive from equation 2, the resonance frequency of the n^{th} mode of vibration of the suspended TiO_2 nanotube as [34]:

$$f_n = \frac{(k_n L)^2}{4\pi L^2} \sqrt{\frac{E(R_o^2 + R_i^2)}{\rho}} \quad (3)$$

Then measuring the modal vibration response is possible to indirectly estimate the Young's modulus of the NTs as:

$$E = \left(\frac{4\pi L^2}{(k_n L)^2} \right)^2 \frac{f_n^2 \rho}{(R_o^2 + R_i^2)} \quad (4)$$

From the measurement of the resonance frequencies and the geometrical features of the suspended TiO_2 nanotubes (frequency dispersion presented in the S.I.), the Young's modulus was extracted with equation (4). A linear dependence of the stiffness of the nanotubes on the annealing temperature was found, with a variation from 57 GPa on the as-synthesized samples to 105 GPa on the samples treated at 600°C (Figure 2b). As expected both values are considerably below the bulky value of 282 GPa [31]. Annealing of the samples induces significantly transformation of the single nanotubes, because of both degradation organic synthesis residual products and crystallization of the samples. The Young's modulus of the single nanostructures were compared with the Young's modulus values of titanium nanotubes array sample investigated with nanoindentation approach (data from [31]). Even if the data were in the same range, the measurements performed with the vibration analysis returned less scattered values, because they are related to single nanotubes and they are not dependent on the bond among close-packed NTs like in the array. Besides, vibrational

measurements represent a non-invasive and non-destructive approach, which, with respect to nanoindentation tests, removes the possibility of artifacts related to the tip by feedback control.

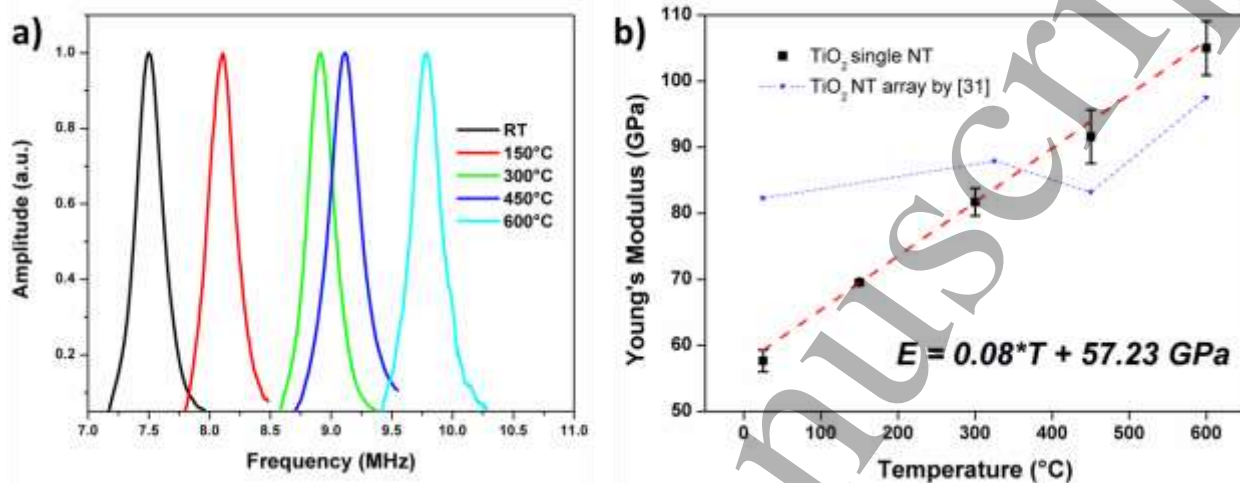


Figure 2. Nanomechanical analysis of suspended nanotubes. (a) Evolution of the first resonance mode of a suspended TiO₂ nanotube after each heating step. The amplitude of the vibration spectra was normalized for a better comparison. (b) Young's modulus of single TiO₂ nanotubes as function of heating step. Star represented literature value from [31] of Young's modulus of TiO₂ nanotube array after different heating treatment

In order to explain the single TiO₂ nanotube transformation induced by thermal annealing and the impact on their mechanical properties, chemico-physical characterizations were performed.

As-synthesized TiO₂ nanotubes, detached from the titanium foil, were tested by means of differential scanning calorimetry (DSC) and thermogravimetric analysis (TGA) analysis. Both the analyses were performed with the same thermal treatment used for the individual suspended nanotubes. DSC analysis showed the presence of two exothermic peaks, centered at 255°C and at 363°C (Figure 3a). The first one can be ascribed to the evaporation of the glycolated species formed in the reaction between oxidized titanium and ethylene glycol; [37] consequently in TGA (Figure 3b) we evidenced a first weight loss (around 1%). The second one could be attributed both to the

thermal crystallization of amorphous phase to anatase[38] and to dehydroxylation of TiOH to TiO₂. [39] Condensation of hydroxyl groups led to a more important weight loss (around 5%), as shown by TGA experiments. These results are in good agreement with what reported in literature, however Raman experiments were performed in over to get more detailed information regarding crystalline phase.

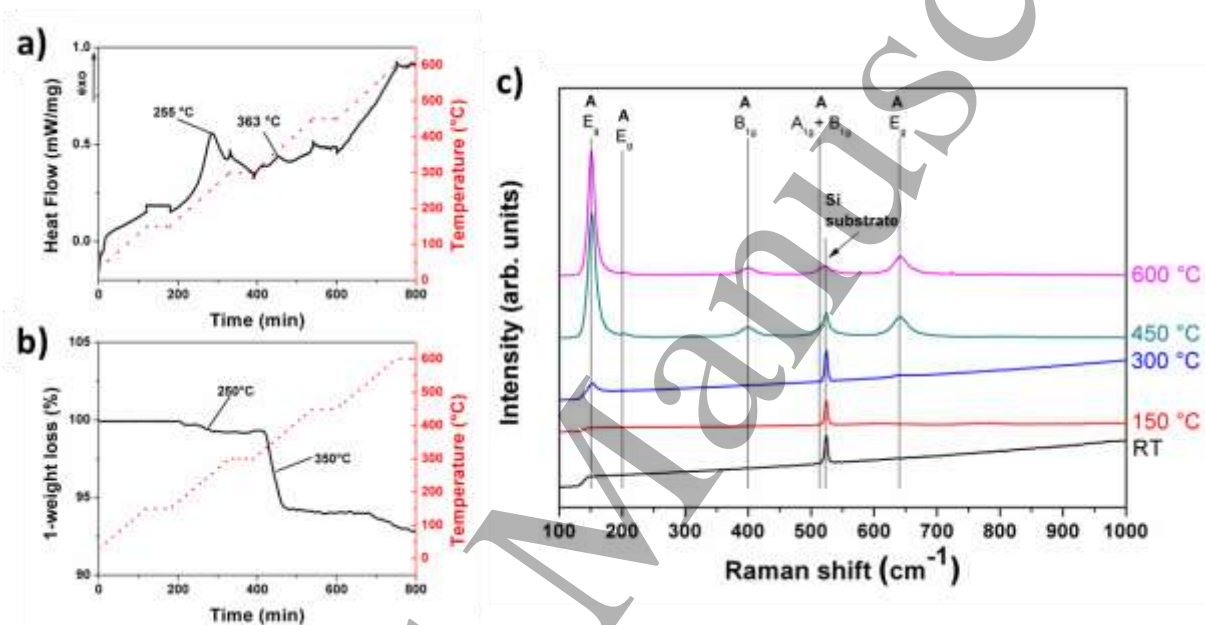


Figure 3. Thermal evolution of titania nanotubes (a) DSC thermogram, (b) TGA analysis and (c) Raman characterization of TiO₂ nanotubes treated at different thermal annealing steps. The five resonances are related with anatase crystalline structure, showing the evolution of the crystallization process. The peak at 520 cm⁻¹ is associated with the silicon substrate.

For mid temperature thermal processes, TiO₂ crystallizes in the anatase phase, which is tetragonal (space group I4₁/amd (No. 141)) with two formula units per unit cell and six Raman active modes (A_{1g}+2B_{1g}+3E_g)[40]. Raman spectra acquired on single nanotubes are collected in Figure 3c, showing resonances at 144 cm⁻¹ (E_g), 197 cm⁻¹ (E_g), 399 cm⁻¹ (B_{1g}), 516 cm⁻¹ (A_{1g} + B_{1g}), and 639 cm⁻¹ (E_g). The crystallization of the structure in the anatase phase has an onset for a temperature lower

1
2
3 than 300 °C. The peak profile at 144 cm⁻¹ becomes sharper during thermal treatment, witnessing the
4 evolution of the crystallinity of the nanotubular structure and the crystalline domains size increase.
5
6
7 No rutile phase is revealed for the performed treatment. This result is in agreement with previous
8 findings[41] that evidenced the formation of rutile nanocrystal for temperature around 500 °C,
9 starting at the interfacial region between nanotubes and growth substrate, for tubular structure
10 synthesized with ethylene glycol based electrolytes. In our case, since the crystallization occurs for
11 single nanotubes or bundles of few nanotubes already detached from the growth substrate, the
12 crystallization dynamics is slower, and rutile formation is expected to occur for temperature higher
13 than 600 °C.
14
15
16
17
18
19
20
21
22
23

24 High resolution TEM (HRTEM) imaging and related analysis, which gives more detailed
25 information on the crystal evolution of the individual titanium dioxide nanotubes, showed result in
26 agreement with what reported above. The structural evolution of TiO₂ amorphous nanotubes (NTs)
27 vs. temperature was studied by HRTEM, using an ex situ approach with the aim of assessing the
28 detailed structural evolution of the sample caused by heating performed in air (see Methods for
29 details). This choice was preferred to the in situ heating approach of TEM experiments, because it
30 granted a straightforward comparison to the above presented characterizations despite its
31 shortcomings, namely the increased stress caused to the thin film of the in situ TEM MEMS and the
32 gradual accumulation of external carbonaceous layer due to the contamination occurring during the
33 heating in air and over the whole sample surface. This additional layer reacted when exposed to the
34 electron beam and accumulated at the border of the areas investigated by HRTEM (as shown by the
35 darker zones in Figure 4b,c), but did not affect in a major way the possibility to carry on the
36 structural analysis of the NTs.
37
38
39
40
41
42
43
44
45
46
47
48
49
50
51
52
53

54 The first evidence of structural evolution was observed after the sample was heated to 150°C, with a
55 minor number of crystalline seeds appearing within the overall amorphous NTs. The seeds were
56 generally small-sized (2÷3 nm-wide), seldom reaching 10 nm. All the seeds displayed
57 monocrystalline features, with interplanar distances and related angular relationships obtained by
58
59
60

1
2
3 HRTEM analysis being compatible with anatase (JCPDS Card No 84-1286, Figure 4d). Heating to
4
5 300°C did not cause major variations in the size of the seeds, although a texturing of the NTs could
6
7 be observed. However, HRTEM analysis showed that at this stage the small (i.e. 2÷3 nm) and big
8
9 (i.e. 10 nm) seeds were still monocrystalline but exhibited diverse interplanar distances and angular
10
11 relationships, with the structural features of the larger seeds being typical of the anatase, and those
12
13 of the smaller ones being consistent with the presence of brookite (JCPDS Card No 76-1937 Figure
14
15 4e). Heating up to 450°C determined a ubiquitous crystallization of the NTs. The increase in
16
17 temperature led to the formation of extended crystalline domains, several tens of nm wide, paired
18
19 with heavily inhomogeneous regions featuring several small crystalline domains. Structural analysis
20
21 confirmed the presence of anatase and brookite in both types of crystalline domains (small and
22
23 extended). Then, despite each phase prevailing over the other one on a local scale, neither of them
24
25 could be indicated as the primary phase on a general term (Figure 4f). However, given the
26
27 intrinsically averaged nature of the Raman technique, the clear presence of the sole anatase
28
29 vibrational peaks indicates that anatase is indeed the primary phase at 300°C.
30
31
32
33
34

35 The chemico-physical characterization performed on individual titanium dioxide nanotubes
36
37 confirmed that their nanomechanical properties are strongly dependent on their crystal evolution
38
39 upon thermal treatment. The almost linearly increase of the Young's modulus can be ascribable to
40
41 two phases. Below 300°C the increasing of elastic modulus is mainly related to the thermal
42
43 decomposition of chemical residual from the synthesis batch (mainly glycolated species) and
44
45 surface trapped water evaporation. These processes harden the nanotubes and thus cause an
46
47 increasing of the resonance frequency. HRTEM analysis also shows the formation of few small
48
49 crystalline seeds (2-3 nm) which, given their scarcity, do not impact the overall amorphous nature
50
51 of the nanotubes. Above 300°C the stiffening of the nanotubes is ascribable firstly to the
52
53 dehydroxylation of TiOH to TiO₂ and then to the crystallization of the titanium dioxide from the
54
55 amorphous form into anatase (with a very low content of brookite) which increases according with
56
57 the temperature of the thermal treatment.
58
59
60

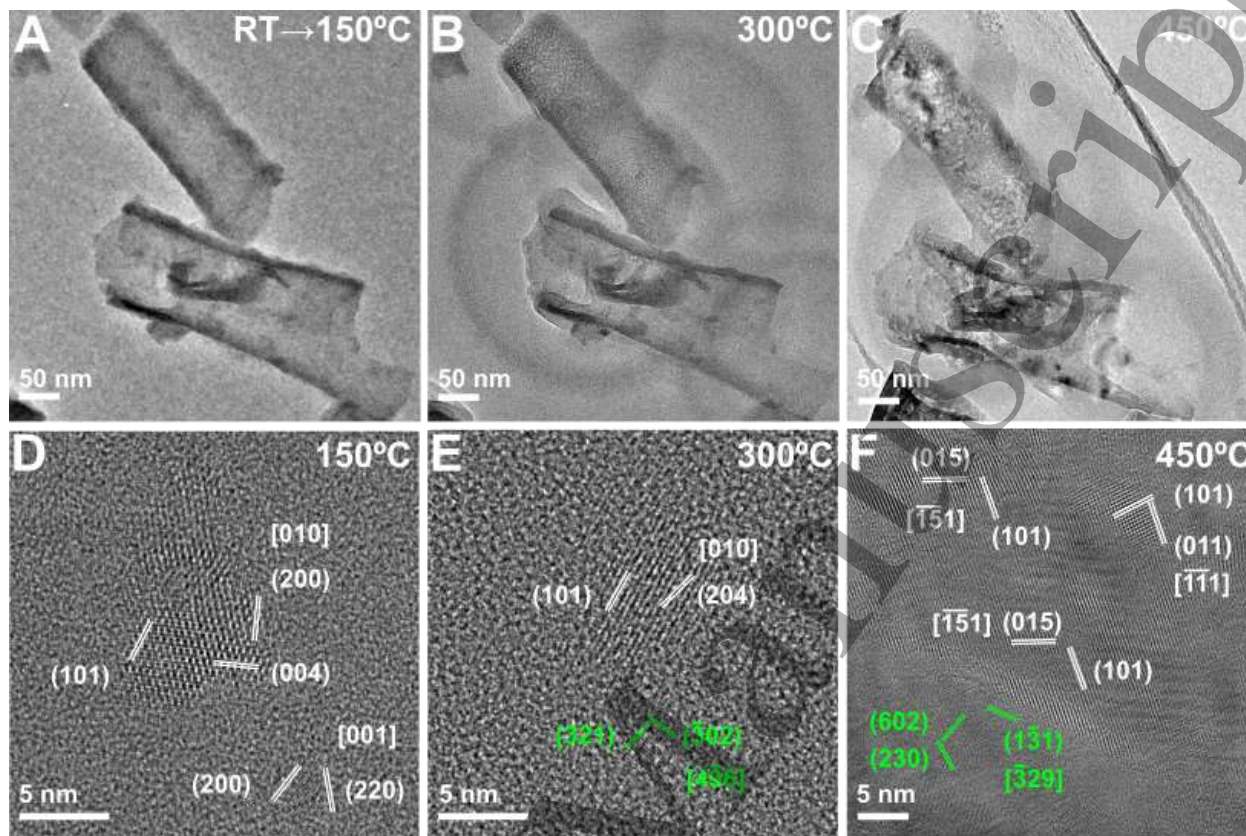


Figure 4 Crystallographic evolution of single TiO₂ nanotubes. (a-c) Low magnification TEM images showcasing the NTs evolution vs. T of the TiO₂ NTs after ex situ heating from RT to 150°C (a), 300°C (b) and 450°C (c); HRTEM images of representative TiO₂ NTs after ex situ heating up to 150°C (d), 300°C (e) and 450°C (f). The structural information on crystalline domains of anatase and brookite are indicated in white and green color, respectively.

CONCLUSION

Nanomechanical properties of individual titanium dioxide nanotubes were studied with a non-invasive indirect approach based on modal vibration response analysis. From the measure of the resonance frequency modes of the suspended nanotubes it was possible to obtain the Young's modulus, which corresponds to 57 GPa for as synthesized nanostructures. Upon thermal treatment the Young's modulus was found to linearly increase up to 105 GPa for 600°C. Chemico-physical

1
2
3 characterizations evidences that below 300°C the stiffening of the nanotubes is induced by organic
4
5 compounds removal trapped from the synthesis process. Above it, the increasing of Young's
6
7 modulus is determined by the crystallization of the TiO₂ nanotubes from the amorphous phase to the
8
9 anatase one. These results give a deeper comprehension of the mechanical properties and
10
11 crystallization evolution of individual titanium dioxide nanotubes extrapolated from their standard
12
13 arrayed architecture. Considering the growing application of nanomaterials, this work provides new
14
15 insights for improved design and understanding of single nanostructure devices.
16
17
18
19
20
21
22

23 CONFLICTS OF INTEREST

24
25
26 The authors declare no competing financial interests.
27
28
29
30
31

32 REFERENCES

- 33
34
35 [1] Gong D, Grimes C A, Varghese O K, Hu W, Singh R S, Chen Z and Dickey E C 2001 Titanium oxide
36 nanotube arrays prepared by anodic oxidation *J. Mater. Res.* **16** 3331-4
37 [2] Bella F, Lamberti A, Bianco S, Tresso E, Gerbaldi C and Pirri C F 2016 Floating, Flexible Polymeric
38 Dye-Sensitized Solar-Cell Architecture: The Way of Near-Future Photovoltaics *Advanced Materials*
39 *Technologies* **1** 1600002
40 [3] Lamberti A, Sacco A, Bianco S, Manfredi D, Cappelluti F, Hernandez S, Quaglio M and Pirri C F 2013
41 Charge transport improvement employing TiO₂ nanotube arrays as front-side illuminated dye-
42 sensitized solar cell photoanodes *PCCP* **15** 2596-602
43 [4] Shankar K, Mor G K, Prakasam H E, Varghese O K and Grimes C A 2007 Self-assembled hybrid
44 polymer-TiO₂ nanotube array heterojunction solar cells *Langmuir* **23** 12445-9
45 [5] Wang X, Li Z, Xu W, Kulkarni S A, Batabyal S K, Zhang S, Cao A and Wong L H 2015 TiO₂ nanotube
46 arrays based flexible perovskite solar cells with transparent carbon nanotube electrode *Nano*
47 *Energy* **11** 728-35
48 [6] Gui Q, Xu Z, Zhang H, Cheng C, Zhu X, Yin M, Song Y, Lu L, Chen X and Li D 2014 Enhanced
49 photoelectrochemical water splitting performance of anodic TiO₂ Nanotube arrays by surface
50 passivation *ACS Applied Materials and Interfaces* **6** 17053-8
51 [7] Hernández S, Hidalgo D, Sacco A, Chiodoni A, Lamberti A, Cauda V, Tresso E and Saracco G 2015
52 Comparison of photocatalytic and transport properties of TiO₂ and ZnO nanostructures for solar-
53 driven water splitting *PCCP* **17** 7775-86
54 [8] Lamberti A, Garino N, Sacco A, Bianco S, Chiodoni A and Gerbaldi C 2015 As-grown vertically
55 aligned amorphous TiO₂ nanotube arrays as high-rate Li-based micro-battery anodes with improved
56 long-term performance *Electrochim. Acta* **151** 222-9
57 [9] Lu X, Wang G, Zhai T, Yu M, Gan J, Tong Y and Li Y 2012 Hydrogenated TiO₂ nanotube arrays for
58 supercapacitors *Nano Lett.* **12** 1690-6
59
60

1
2
3
4
5
6
7
8
9
10
11
12
13
14
15
16
17
18
19
20
21
22
23
24
25
26
27
28
29
30
31
32
33
34
35
36
37
38
39
40
41
42
43
44
45
46
47
48
49
50
51
52
53
54
55
56
57
58
59
60

- [10] Zou J, Zhang Q, Huang K and Marzari N 2010 Ultraviolet photodetectors based on anodic TiO₂ nanotube arrays *Journal of Physical Chemistry C* **114** 10725-9
- [11] Lamberti A, Virga A, Chiadò A, Chiodoni A, Bejtka K, Rivolo P and Giorgis F 2015 Ultrasensitive Ag-coated TiO₂ nanotube arrays for flexible SERS-based optofluidic devices *Journal of Materials Chemistry C* **3** 6868-75
- [12] Mor G K, Carvalho M A, Varghese O K, Pishko M V and Grimes C A 2004 A room-temperature TiO₂-nanotube hydrogen sensor able to self-clean photoactively from environmental contamination *J. Mater. Res.* **19** 628-34
- [13] Berger S, Ghicov A, Nah Y C and Schmuki P 2009 Transparent TiO₂ nanotube electrodes via thin layer anodization: Fabrication and use in electrochromic devices *Langmuir* **25** 4841-4
- [14] Liu Z, Zhang X, Nishimoto S, Jin M, Tryk D A, Murakami T and Fujishima A 2008 Highly ordered TiO₂ nanotube arrays with controllable length for photoelectrocatalytic degradation of phenol *Journal of Physical Chemistry C* **112** 253-9
- [15] Conti D, Lamberti A, Porro S, Rivolo P, Chiolerio A, Pirri C F and Ricciardi C 2016 Memristive behaviour in poly-acrylic acid coated TiO₂ nanotube arrays *Nanotechnology* **27** 485208
- [16] Park J, Bauer S, Von Der Mark K and Schmuki P 2007 Nanosize and vitality: TiO₂ nanotube diameter directs cell fate *Nano Lett.* **7** 1686-91
- [17] Chiarello G L, Zuliani A, Ceresoli D, Martinazzo R and Selli E 2016 Exploiting the Photonic Crystal Properties of TiO₂ Nanotube Arrays to Enhance Photocatalytic Hydrogen Production *ACS Catalysis* **6** 1345-53
- [18] Roy P, Berger S and Schmuki P 2011 TiO₂ nanotubes: Synthesis and applications *Angewandte Chemie - International Edition* **50** 2904-39
- [19] Yu J, Dai G and Cheng B 2010 Effect of crystallization methods on morphology and photocatalytic activity of anodized TiO₂ nanotube array films *Journal of Physical Chemistry C* **114** 19378-85
- [20] Lamberti A, Chiodoni A, Shahzad N, Bianco S, Quaglio M and Pirri C F 2015 Ultrafast room-temperature crystallization of TiO₂ nanotubes exploiting water-vapor treatment *Scientific Reports* **5** 7808
- [21] Kim Y H, Heo J S, Kim T H, Park S, Yoon M H, Kim J, Oh M S, Yi G R, Noh Y Y and Park S K 2012 Flexible metal-oxide devices made by room-temperature photochemical activation of sol-gel films *Nature* **489** 128-32
- [22] Bella F, Lamberti A, Sacco A, Bianco S, Chiodoni A and Bongiovanni R 2014 Novel electrode and electrolyte membranes: Towards flexible dye-sensitized solar cell combining vertically aligned TiO₂ nanotube array and light-cured polymer network *Journal of Membrane Science* **470** 125-31
- [23] Lamberti A, Fontana M, Bianco S and Tresso E 2016 Flexible solid-state Cu_xO-based pseudo-supercapacitor by thermal oxidation of copper foils *Int. J. Hydrogen Energy* **41** 11700-8
- [24] Li M, Mayer T S, Siooss J A, Keating C D and Bhiladvala R B 2007 Template-grown metal nanowires as resonators: Performance and characterization of dissipative and elastic properties *Nano Lett.* **7** 3281-4
- [25] Eom K, Park H S, Yoon D S and Kwon T 2011 Nanomechanical resonators and their applications in biological/chemical detection: Nanomechanics principles *Physics Reports* **503** 115-63
- [26] Xu Y N, Liu M N, Wang M C, Oloyede A, Bell J M and Yan C 2015 Nanoindentation study of the mechanical behavior of TiO₂ nanotube arrays *J. Appl. Phys.* **118** 145301
- [27] Santos L S, Oliveira N T C, Lepienski C M, Marino C E B and Kuromoto N K 2014 Elastic modulus evaluation of titania nanotubes obtained by anodic oxidation *Revista Materia* **19** 33-9
- [28] Crawford G A, Chawla N, Das K, Bose S and Bandyopadhyay A 2007 Microstructure and deformation behavior of biocompatible TiO₂ nanotubes on titanium substrate *Acta Biomaterialia* **3** 359-67
- [29] Chang W Y, Fang T H, Chiu Z W, Hsiao Y J and Ji L W 2011 Nanomechanical properties of array TiO₂ nanotubes *Microporous Mesoporous Mater.* **145** 87-92
- [30] Hirakata H, Ito K, Yonezu A, Tsuchiya H, Fujimoto S and Minoshima K 2010 Strength of self-organized TiO₂ nanotube arrays *Acta Mater.* **58** 4956-67
- [31] Munirathinam B and Neelakantan L 2016 Role of crystallinity on the nanomechanical and electrochemical properties of TiO₂ nanotubes *J. Electroanal. Chem.* **770** 73-83

- 1
2
3 [32] Shokuhfar T, Arumugam G K, Heiden P A, Yassar R S and Friedrich C 2009 Direct compressive
4 measurements of individual titanium dioxide nanotubes *ACS Nano* **3** 3098-102
5 [33] Kang S H, Fang T H, Chen T H, Hsiao Y J, Hong Z H, Chuang C H and Riccobono L 2014 Size effect on
6 mechanical properties of TiO₂ capped nanotubes investigated using in situ transmission electron
7 microscopy *Microsystem Technologies* **20** 515-20
8 [34] Treacy M M J, Ebbesen T W and Gibson J M 1996 Exceptionally high Young's modulus observed for
9 individual carbon nanotubes *Nature* **381** 678-80
10 [35] Stassi S, Cauda V, Fiorilli S and Ricciardi C 2015 Surface area enhancement by mesoporous silica
11 deposition on microcantilever sensors for small molecule detection *Journal of Materials Chemistry*
12 *C* **3** 12507-13
13 [36] Stassi S, Chiadò A, Calafiore G, Palmara G, Cabrini S and Ricciardi C 2017 Experimental evidence of
14 Fano resonances in nanomechanical resonators *Scientific Reports* **7** 1065
15 [37] Jiang X, Herricks T and Xia Y 2003 Monodispersed spherical colloids of titania: Synthesis,
16 characterization, and crystallization *Adv. Mater.* **15** 1205-9
17 [38] Oh H-J, Lee S, Lee B, Jeong Y and Chi C-S 2011 Surface characteristics and phase transformation of
18 highly ordered TiO₂ nanotubes *Metals and Materials International* **17** 613
19 [39] Del Ángel-Sánchez K, Vázquez-Cuchillo O, Salazar-Villanueva M, Sánchez-Ramírez J F, Cruz-López A
20 and Aguilar-Elguezabal A 2011 Preparation, characterization and photocatalytic properties of TiO₂
21 nanostructured spheres synthesized by the Sol-Gel method modified with ethylene glycol *J. Sol-Gel*
22 *Sci. Technol.* **58** 360-5
23 [40] Bersani D, Lottici P P and Ding X Z 1998 Phonon confinement effects in the Raman scattering by
24 TiO₂ nanocrystals *Appl. Phys. Lett.* **72** 73-5
25 [41] Jarosz M, Syrek K, Kapusta-Kołodziej J, Mech J, Matek K, Hnida K, Łojewski T, Jaskuła M and Sulka G
26 D 2015 Heat treatment effect on crystalline structure and photoelectrochemical properties of
27 anodic TiO₂ nanotube arrays formed in ethylene glycol and glycerol based electrolytes *Journal of*
28 *Physical Chemistry C* **119** 24182-91
29
30
31
32
33
34
35
36
37
38
39
40
41
42
43
44
45
46
47
48
49
50
51
52
53
54
55
56
57
58
59
60